Geoderma 411 (2022) 115712

Contents lists available at ScienceDirect

Geoderma

journal homepage: www.elsevier.com/locate/geoderma

Unequal weakening of urbanization and soil salinization on vegetation production capacity

Qingwei Zhuang [a], Zhenfeng Shao [a,*], Deren Li [a,b], Xiao Huang [c], Bowen Cai [b], Orhan Altan [d], Shixin Wu [e]

[a] State Key Laboratory of Information Engineering in Surveying, Mapping and Remote Sensing, Wuhan University, Wuhan 430079, China
[b] School of Remote Sensing and Information Engineering, Wuhan University, Wuhan 430079, China
[c] Department of Geosciences, University of Arkansas, Fayetteville, AR 72701, USA
[d] Department of Geomatics Engineering, Istanbul Technical University, Istanbul 36626, Turkey
[e] State Key Laboratory of Desert and Oasis Ecology, Xinjiang Institute of Ecology and Geography, Chinese Academy of Sciences, Urumqi 830011, China

ARTICLE INFO

Handling Editor: Ingrid Kögel-Knabner

Keywords:
Climate change
Urbanization
Soil salinization
Agricultural management practices
NPP
Farmland ecosystem

ABSTRACT

Net Primary Productivity (NPP) has been widely used to estimate the productivity of the farmland ecosystem (FES) and the carbon budget of the terrestrial ecosystem. Changes in the NPP of FES have knock-on effects on food security, sustainable agricultural development, carbon sequestration, and environmental changes. Existing studies mainly focused on the impact of climate change and urbanization on the spatial-temporal pattern of NPP, largely ignoring the roles of soil condition and agricultural management practices (AMPs). At present, the joint impact of "climate-urbanization-soil-AMPs" on the NPP of FES remains unknown. To fill this knowledge gap, we use the NPP dataset retrieved by the vegetation photosynthesis model (VPM), daily meteorological records, field-collected soil data, AMPs data collected from the Government Statistical Yearbook, and land cover dataset to study the joint mechanism of "climate-urbanization-soil" that drives spatial-temporal variations of NPP. Taking the northern slope of Tianshan Mountains as the study area, our results indicate that NPP had increased by 3.86 Tg C from 2000 to 2015 (11.93 Tg C in 2000 and 15.79 Tg C in 2015). From the proposed conceptual framework, we found that climate variables (accumulated temperature, precipitation, evapotranspiration) play a major role in driving the growth of NPP (+4.01 Tg C). The AMPs (i.e., mulching filming, drip irrigation, and fertilizer application) make a positive contribution to NPP increase (+0.98 Tg C). We also found that soil salinization (-1.07 Tg C) weakens the growth of NPP more significantly than urbanization (−0.16 Tg C). This study provides new insights on the mechanism of climate change, urbanization, and soil conditions on crops, benefiting stakeholders in designing better management plans for sustainable agriculture, ecosystem cycling, and food security.

1. Introduction

As an important part of terrestrial ecosystems, the farmland ecosystem (FES) plays an important role in regional climate change and global carbon cycle (Brandt et al., 2018; Luo et al., 2018). Net Primary Productivity (NPP) refers to the total amount of organic matter accumulated by green vegetation during photosynthesis per unit time and area (Field et al., 1995; He et al., 2017; Jiang et al., 2020). It is an important ecological indicator that avoids the interference caused by the adjustment of agricultural structure and the change of crop varieties (Stocker et al., 2019; Salas, 2020). Especially, the world is on the verge of the worst food crisis in at least 50 years (Asiedu et al., 2020). Nearly 690 million people suffered from hunger in 2019, an increase of 10 million compared with 2018 and an increase of nearly 60 million compared with 2014 (FAO, 2020). Kansiime et al. (2021) estimated that an additional 130 million more people would be chronically hungry due to the Coronavirus Disease 2019 (COVID-19) and African locust plague at the end of 2020. In the context of the global food crisis, scientific exploration of the spatiotemporal changing mechanism of NPP in FES contributes to a better understanding of climate change, terrestrial carbon budget assessment, and food security.

In the existing literature of NPP, more attention was paid to

* Corresponding author.
E-mail address: shaozhenfeng@whu.edu.cn (Z. Shao).

https://doi.org/10.1016/j.geoderma.2022.115712
Received 16 August 2021; Received in revised form 22 December 2021; Accepted 8 January 2022
Available online 20 January 2022

vegetation changes in natural ecosystems (i.e., forests and grasslands) (Doughty et al., 2015; Ghiloufi and Chaieb, 2021; Huang et al., 2018; Jones et al., 2020; Liu et al., 2018). In contrast, NPP changes in FES received little attention. Some studies only focus on the impact of urbanization or climate change on farmland NPP, ignoring soil and agricultural management practices (AMPs). The spatial–temporal responses of NPP to the combined effects of "climate - urbanization - soil - AMPs" thus remain underexploited, leading to a gap that can be filled to better understand the changing mechanism of the carbon cycle in farmland ecosystems. Filling this knowledge gap also benefits decision-makers in determining effective mitigation and adaptation strategies to enhance farmland ecosystems' response to food crisis capacity and adaptability to future environmental changes.

The impacts of global climate change on NPP in the natural ecosystem have been well documented in the existing literature. A general consensus is that global climate warming is likely to boost the NPP of natural vegetation. Liu et al. (2018) found the ecosystems of extensive soil carbon stocks alpine grassland are largely shaped by temperature. Doughty et al. (2015) documented drought inhibits forest carbon dynamics and fluxes in Amazonia. Studies found that factors that include interannual variabilities of temperature, precipitation, and extreme weather events are most likely to impact the shifts of natural NPP (Huang et al., 2019; Kong et al., 2019; Pan and Dong 2018; Shao et al. 2017). However, as a semi-natural and semi-artificial ecosystem, the changing mechanism of NPP in FES is more complicated (Le Noë et al., 2019; Niu et al., 2016) without a clear explanation (Weinzettel et al., 2019), thus deserving further investigation.

Recently, there has been a growing interest that focuses on the impact of urbanization on vegetation productivity (Buyantuyev and Wu 2009; d'Amour et al., 2017; Dong et al., 2015; He et al., 2017; Li et al., 2016; Liu et al., 2019a). Many studies have shown that a large amount of agricultural land has been transformed into impervious surfaces (e.g., roads, houses, and buildings) during the decades of urbanization (Nuarsa et al., 2018; Shao and Lunetta 2012; Shao et al., 2020; Wen et al., 2019; Wu et al., 2014). Meanwhile, the vegetation growth environment (e.g., climate, soil texture, and atmospheric conditions) is also severely affected by the urbanization process (Gregg et al., 2003; McCubbin et al., 2015; Miller and Hutchins 2017; Tran et al., 2017). In addition to urbanization, AMPs may have a positive impact on farmland NPP. Therefore, some studies that investigated land use/ cover change (LUCC) with human activities have certain limitations. Existing efforts have paid more attention to the role played by agricultural management practices in increasing the NPP of terrestrial ecosystems. Agricultural management changes NPP by affecting soil aggregates and C protection in aggregates pointed out that different agronomic managements have different effects on the distribution and stability of aggregation. In recent years, AMPs in arid regions have undergone tremendous changes, reflected from three aspects: mulching farming, drip irrigation, and fertilizer application. In this study, we argue that it is necessary to dialectically explore the impact of human activities on farmland NPP.

Soil salinization, as a key indicator of soil conditions, has attracted wide attention from many scholars (Dehaan and Taylor 2002; Khongnawang et al., 2020; Muyen et al., 2011). The arid region accounts for 41% of the world's land area and feeds 38% of the world's population (Jiang et al., 2019). In general, soil salinization is worse in arid regions, as 30% of the irrigated agriculture is in saline (Daliakopoulos et al., 2016; Farzamian et al., 2019; Islam et al., 2019). It has become an important factor that restricts the growth of crops, posing challenges to sustainable agricultural development. Therefore, the investigation of the impact of climate change, urbanization, AMPs, and soil salinization on farmland NPP and the distinguishment of their respective contributions are essential for a comprehensive understanding of the systemic impact of natural and human factors on farmland NPP.

If agricultural management practices (AMPs) continue to be improved with warmer and more humid climates (excluding extreme climates), the NPP of crops in arid areas is expected to increase. Nevertheless, we suspect that urbanization and soil salinization can slow down or even hinder this progress. To prove this hypothesis, we explored the combined effects of climate change, urbanization, soil salinization, and AMPs on the NPP in arid FES. We chose the northern slope of Tianshan Mountain as the study area because it is the largest urban agglomeration in Central Asia, characterized by the fastest urbanization rate and a large-scale agricultural ecosystem. Specifically, we seek to answer the following questions: (1) How did the NPP of the farmland ecosystem change from 2000 to 2015? (2) How much of those variations can be attributed to climate variables (i.e., accumulated temperature (AT), accumulated precipitation (AP), and evapotranspiration (ET)), urbanization (impervious surface area), soil salinization, and AMPs (i.e., mulching filming, drip irrigation, and fertilizer application), respectively? We conducted a comprehensive assessment of the temporal and spatial variability of agricultural ecosystems, contributing to the essential knowledge that is expected to benefit the sustainable development of agriculture and the response to food crises.

2. Materials and methods

2.1. Study area

The northern slope of Tianshan Mountains, covering a total area of 14.66×10^4 km^2 (accounting for 8.78% of Xinjiang Province), refers to a long and narrow area along the Tianshan Mountains at 42°50′N–46°12′N and 79°53′E–92°06′E (Fig. 1). It is one of the 12 national cities in China and plays an important role in The Belt and Road. It is located in the hinterland of the Eurasian continent, far away from the ocean. Its climate is featured by cold and long winter, hot and dry summer, and large day-night temperature differences. The annual average precipitation, mainly concentrated in May and June, is between 150.13 and 360.81 mm. The annual average temperature is between 4.5 and 7.0 °C in the study area (highest in July at 23.7 °C, lowest in January at −10.4 °C). Tianshan Mountains, as one of the huge mountain series in Central Asia, span many countries. The northern slope of Tianshan Mountains is mainly composed of Jurassic strata, and the front mountains and low hills are mainly covered by loess. There exists severe soil salinization in the irrigation area, posing great threats to local food security. Meanwhile, the rapid urbanization in the study are is likely to encroach on cultivated land resources. In light of such background of landscape patterns, we decided to use it as our study area.

2.2. Data

2.2.1. Net primary productivity (NPP) retrieval

We selected the vegetation photosynthesis model (VPM), a light energy utilization model, to simulate the NPP at a temporal resolution of 8 days. Compared with other NPP estimation models, VPM has several merits, such as concise input parameters, high accuracy, and fast calculation (Pei et al., 2020; Walther et al., 2016). The details of VPM are shown in Table S1. The spatial resolution of the derived NPP dataset is 500 m*500 m. To confine all data to a consistent spatial resolution, we further interpolated the NPP dataset to a spatial resolution of 30 m*30 m via an Ordinary Kriging method.

2.2.2. Soil sampling and mapping soil salinization in arid FES

According to soil type, crop type, soil parent material and cultivated land reclamation period, arrange representative cultivated land sampling points on the high-resolution topographic map, and master the spatial distribution of the sampling points, using GPS positioning to select a total of 73 in the Sangong river basin representative sampling points (Fig. 1), and soil sampling will be carried out in May 2005 and May 2014 (not-crop growth period). When sampling, the ridge roadsides, ditches, micro-topography, etc. were avoided, a composite soil sample from each plot was collected by combining six randomly collected cores from soybean inter-row from 0 − 30 cm depth using a

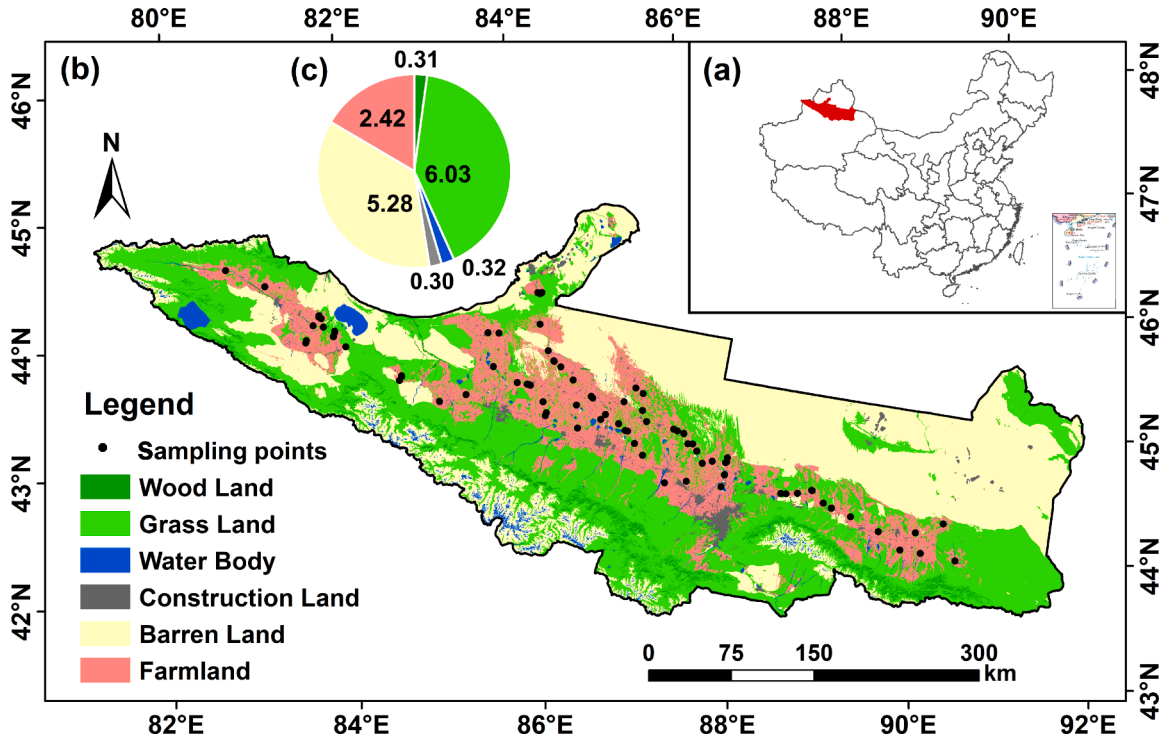

Fig. 1. (a) Location of the northern slopes of Tianshan Mountains in China; (b) Distribution of sampling points and land use types of the study area; (c) Composition of land use type in the study area (unit: 104 km2).

bucket type auger of 5 cm diameter. A part of the soil sample was air-dried and passed through an 8 mm sieve to collect samples for aggregate size distribution and stability analyses, and another part was passed through a 2 mm sieve for bulk-soil analysis. The test methods and results can be found in Table S2.

Based on the classification system of soil salinization in the second soil survey in Xinjiang Province, we established an analytical method based on the analytic hierarchy process (AHP) to investigate soil salinization in the irrigated northern slopes of Tianshan Mountains (Zhuang et al., 2021). In the process of constructing the AHP method, the selection of evaluation indicators is the most important step. We used principal component analysis to select four factors (i.e., TS, pH,Cl^-, andSO_4^{2-}) that have the greatest impact on soil salinization from a total of nine soil factors derived from the laboratory experiments (Table 1). These 4 factors aim to express the natural conditions of the cultivated land. It is widely acknowledged that there exists an interactive relationship between the degree of soil salinization and crop production capacity. We used the digital elevation model (DEM) and slope to express the natural conditions of cultivated land, given the fact that natural conditions of cultivated land also have a great influence on soil salinization. DEM and slope data were collected from the Resource Environmental Science and Data Center, Chinese Academy of Sciences (http://www.resdc.cn). To analyze the distribution of soil salinization more precisely, we divided soil salinization into four levels according to the score. The specific grading standards were as follows: [0, 25] is defined as severe salinization; (25, 50] is defined as moderate salinization; (50, 75] is defined as mild salinization; (75, 100] is defined as none salinization.

2.2.3. Climate dataset

We selected accumulated temperature (AT), accumulated precipitation (AP), and evapotranspiration (ET) to investigate how climatic variables influence NPP in the arid farmland ecosystem. Those climatic variables have been widely used to explain the spatiotemporal variations of NPP (Alton 2020; Chen et al., 2013; Li et al., 2020; Tian et al., 2016). AT and AP datasets were obtained from the National Meteorological Information Center of China (http://data.cma.cn/). We derived the gridded climate dataset with a spatial resolution of 1 km*1 km via AUNSPIN, a popular software to analyze and interpolate multivariate data with the capacity to perform statistical analysis, data diagnosis, and spatial interpolation.

Evapotranspiration (ET) is an important component of the land water cycle (Chen et al., 2020). ET dataset (with non-vegetation area excluded) was developed by the Earth Dynamics Numerical Simulation Research Group of the University of Montana at Missoula. The main input variables include meteorological data, fraction of photosynthetically active radiation (FPAR), leaf area index (LAI) dataset, and some auxiliary data. EF is calculated using the Penman-Monteith (P-M)

Table 1
Grading schemes of soil salinization classification indicators.

Guidelines	Indicators	Scoring standard					
		100	80	60	40	20	0
Soil conditions	TS (g/kg)	<3.5	3.5–5.0	5.0–6.0	6.0–8.5	8.5–10.0	>10.0
	pH	<8.0	8.0–8.5	8.5–9.0	9.0–9.5	9.5–10.0	>10.0
	Cl^-(g/kg)	<7.0	7.0–9.0	9.0–13.0	13.0–16.0	16.0–20.0	>20.0
	SO_4^{2-}(g/kg)	<8.0	8.0–10.0	10.0–15.0	15.0–20.0	20.0–25.0	>25.0
Natural indicators	DEM (m)	0–500	500–1,000	1,000–1,500	1,500–2,000	2,000–2,500	>2,500
	Slope (°)	<1.0	1.0–3.0	3.0–5.0	5.0–7.0	7.0–10.0	>10.0

formula based on the principles of energy balance and turbulence diffusion:

$$ET = \frac{sA + \rho C_p(e_{sat} - e)/r_a}{s + \gamma(1 + r_s/r_a)} \quad (1)$$

where S is the slope of the curve of saturated vapor pressure and temperature; A is the available energy; ρ is the air density; C_p is the specific heat of the air at constant pressure; γ is the wet and dry gauge constant; e_{sat} is the saturated vapor pressure; e is the actual vapor pressure; r_a and r_s are aerodynamic impedance and surface impedance, respectively.

2.2.4. Validation dataset

(1) We verified the calculated NPP using measured biomass data. In this study, we conducted a correlation analysis between the measured value of biomass and the NPP obtained by the VPM model inversion. The results show that the simulated value of NPP is considerably consistent with the measured value of NPP ($R^2 = 0.724\ 7$, $P < 0.01$). (2) The land use and land cover dataset with 30 m* 30 m spatial resolution was developed via the Random Forest algorithm, with accuracy verified by the overall accuracy and Kappa coefficient. More details can be found in our previous work (Zhuang et al., 2020). (3) For the soil data, we selected 52 samples (out of a total of 72) for spatial visualization and the remaining 20 samples for verification. The correlation coefficient between the actual values of the verification soil samples and the simulated values is 0.839 ($P < 0.01$). (4) All gridded climate datasets have been verified using data collected from observation sites.

2.3. Statistical analysis

2.3.1. Spatial-temporal dynamics of NPP during 2000–2015

To further analyze the relative contribution of climate and soil salinization to the change of NPP in arid farmland ecosystems, we derived the trend of NPP via linear regression method with time (i.e., year) as the independent variable and corresponding NPP data as the dependent variable. The F-test of the correlation coefficient between the annual cumulative value and the year was used to judge the significance of the annual changing trend of NPP. Similarly, climate change is calculated using the same method. The trend slope of the annual NPP (θ_{slope}) is calculated as:

$$\theta_{\text{slope}} = \frac{n \times \sum_{i=1}^{n} x_i t_i - \sum_{i=1}^{n} x_i \sum_{i=1}^{n} t_i}{n \times \sum_{i=1}^{n} t_i^2 - \left(\sum_{i=1}^{n} t_i\right)^2} \quad (2)$$

where θ_{slope} represents the trend of annual NPP; n represents the total number of years; x_i is the annual NPP in the *i-th* year; t_i is the year code (2000, 2001, …, and 2015 correspond to 1, 2, …, and 16). F-test follows:

$$F = \sum_{i=1}^{n} (\overleftrightarrow{x_i} - \overline{x})^2 \times \frac{n-2}{\sum_{i=1}^{n} (x_i - \overleftrightarrow{x_i})} \quad (3)$$

where n represents the total number of years; x_i is the annual NPP in the *i-th* year; $\overleftrightarrow{x_i}$ is the annual regression NPP in the *i-th* year; $\overline{x}$ refers to mean NPP during the investigated period.

2.3.2. A conceptual framework for quantifying the joint impacts of "climate-urbanization-soil" on NPP

We proposed a conceptual framework to quantify the impacts of "climate-urbanization-soil-AMP" on NPP variations in arid FES, which separated the impacts into respective contributions of climatic variables (*Contr.Cli*), urbanization (*Contr.Urb*), soil salinization (*Contr.Soi*), AMPs (*Contr.Amp*), and residual factors (ε). We applied a total least squares optimal fingerprinting approach that uses a generalized linear regression model to represent observed changes as a linear combination of signals for detection and attribution (Sun et al., 2016). *Contr.Cli* induced by several climatic factors may promote or inhibit the crop production capacity. *Contr.Urb* mainly results from the encroach of arable land by impervious surfaces (IS). *Contr.Soi* induced by some key soil biochemical parameters and environmental parameters is likely to cause the emergence of varying degrees of inhibition in the process of vegetation development. *Contr.Amp* induced by the advances in agricultural management practices. In addition, the productivity of crops is affected by other factors (e.g., crop species, planting system, etc.). The impacts of "climate-urbanization-soil-AMPs" on NPP variations in arid FES is quantified as:

$$\Delta NPP = Contr.Cli + \text{Contr.}Urb + Contr.Soi + Contr.Amp + \varepsilon \quad (4)$$

$$\text{Contr.}Cli = Contr.AP + Contr.AT + Contr.ET \quad (5)$$

$$Contr.AP = \frac{\partial NPP}{\partial AP} \times \frac{\partial AP}{\partial n} \quad (6)$$

$$Contr.AT = \frac{\partial NPP}{\partial AT} \times \frac{\partial AT}{\partial n} \quad (7)$$

$$Contr.ET = \frac{\partial NPP}{\partial ET} \times \frac{\partial ET}{\partial n} \quad (8)$$

where *Contr.AT*, *Contr.AP*, and *Contr.ET* are the contributions of AT, AP, and ET to the inter-annual variability of NPP; $\partial NPP/\partial AT$ is the slope of the linear regression between NPP and AT; $\partial AT/\partial n$ is the slope of the linear regression between AT and n; n is the number of years. The calculations of *Contr.AP* and *Contr.ET* are similar to that of *Contr.AT*.

The NPP dynamics in the urbanization-driven scenario were represented as the slope of the urbanization-driven NPP amount plotted as a function of time, assuming a fixed rate of the urban sprawl during the study period (Eq. (9)):

$$\text{Contr.}Urb = \frac{(NPP_{pre\_Urb} - NPP_{post-Urb})}{\text{n}} \times \Delta A_{IS} \quad (9)$$

where NPP_{pre_Urb} is the pre-urban NPP, NPP_{post_Urb} is the post-urban NPP, n is the total number of years, andΔA_{IS} is the expanded area of IS during the study period.

Agricultural management practices affect the NPP dynamics in the farmland ecosystem. Long-term cropping system experiments offer a great opportunity to understand the magnitude and direction of NPP changes. In recent decades, the changes in agricultural management practices are mainly reflected in mulching planting, drip irrigation technology, and fertilizer application per unit area. The detailed formulas are presented as follows:

$$Contr.Amp = Contr.Mulch + Contr.Drip + Contr.Fertilization \quad (10)$$

$$Contr.Mulch = NPP_{post-mulch} - NPP_{pre-mulch} \quad (11)$$

$$Contr.Drip = NPP_{post-drip} - NPP_{pre-drip} \quad (12)$$

$$Contr.Fertilization = NPP_{post-fertilization} - NPP_{pre-fertilization} \quad (13)$$

where *Contr.Mulch*, *Contr.Drip*, and *Contr.Fertilization* are the contributions of mulching planting, drip irrigation technology, and fertilizer application per unit area to the NPP changes; $NPP_{post\text{-}mulch}$ and $NPP_{pre\text{-}mulch}$ are the average NPP within the post-mulch and pre-mulch periods; $SOC_{post\text{-}drip}$ and $SOC_{pre\text{-}drip}$ represent the average NPP within the post-drip irrigation and pre-drip irrigation periods; $SOC_{post\text{-}fertilization}$ and $SOC_{pre\text{-}fertilization}$ denote the average NPP within the post-fertilization and pre-fertilization periods.

Pixel-wise NPP can be decomposed into contributions from none salinization and salinization. *Contr.Soi* that represents the accumulated deviation caused by salinization is calculated based on the following Equation:

$$Contr.Soi = \Delta NPP_{mild} \times A_{mild} + \Delta NPP_{mod.} \times A_{mod.} + \Delta NPP_{sev.} \times A_{sev.} \quad (14)$$

$$\Delta NPP_{\text{none}} = \overline{NPP_{none}} - \overline{NPP_{FES}} \quad (15)$$

$$\Delta NPP_{mild} = \overline{NPP_{mild}} - \overline{NPP_{FES}} \quad (16)$$

$$\Delta NPP_{mod.} = \overline{NPP_{mod.}} - \overline{NPP_{FES}} \quad (17)$$

$$\Delta NPP_{sev.} = \overline{NPP_{sev.}} - \overline{NPP_{FES}} \quad (18)$$

where $\overline{NPP_{none}}$, $\overline{NPP_{mild}}$, $\overline{NPP_{mod.}}$, and $\overline{NPP_{sev.}}$ are the mean values of NPP in none salinization, mild salinization, moderate salinization, and severe salinization, respectively; A_{mild}, $A_{mod.}$, and $A_{sev.}$ are the areas of none salinization, mild salinization, moderate salinization, and severe salinization in arid farmland ecosystem, respectively.

3. Results

3.1. Interannual variations and spatial–temporal trends of NPP in FES

The spatial distribution of the average annual NPP in the farmland ecosystem from 2000 to 2015 is shown in Fig. 2a. The total amount of NPP ranges from 11.26 Tg C year^{-1} to 14.59 Tg C year^{-1}, with a mean value of 561.72 g C m^{-2} year^{-1} for all 24,246 grid cells. In general, the NPP in the farmland ecosystem shows a notable increasing trend at a rate of 10.62 g C m^{-2} year^{-1} ($R^2 = 0.829$ and $p < 0.01$) (Fig. 2b). The inter-annual NPP fluctuates from 464.55 g C m^{-2} year^{-1} to 698.59 g C m^{-2} year^{-1}. At pixel scale, the results show that 18,624 grid cells (accounting for 76.81% of all grid cells) presented statistically significant increasing trends ($p < 0.05$) (Fig. 2c). Whereas 3,316 grid cells (accounting for 13.68% of all grid cells) presented statistically significant decreasing trends ($p < 0.05$). No obvious trending behavior was found for the remaining 2,306 grid cells.

Spatial-temporal dynamics of variables during 2000–2015

3.1.1. Spatial-temporal heterogeneity of climatic factors in FES

Fig. 3a shows the spatial pattern of AP in FES on the northern slope of the Tianshan Mountains. AP shows a significant increasing trend at 4.13 mm per year ($p > 0.05$), with the largest value occurring in 2015 (305.60 mm) and the smallest in 2008 (153.51 mm). Pixel-scale analysis shows that the area with increased precipitation accounts for 82.46% of the total area (slope > 0), of which the area with a statistically significant increasing trend accounts for 65.55% ($p < 0.05$) (Fig. 3b).

During the investigated period, the average value of AT of FES on the northern slope of Tianshan Mountain ≥ 10 °C was between 1640.65 °C. day and 2395.44 °C. day (Fig. 3c). In general, AT does not increase in a statistically significant manner (only at a rate of 3.14 °C. day per year) ($p > 0.05$). The spatiotemporal trend of AT at pixel-level shows that 72.97% of the pixels exhibit an increasing trend, and the significantly increased pixels account for 66.21% of the total pixels ($p < 0.05$) (Fig. 3d).

Meanwhile, 19.35% of the pixels showed a significant decreasing trend in AT ($p < 0.05$). The multi-year average ET of FES on the northern slope of Tianshan Mountain is 1383.71mmm, ranging from 857.70 mm (occurred in the year 2001) to 1865.34 mm (occurred in the year 2013) (Fig. 3e). Overall, ET in the study area increased significantly at a rate of 53.30 mm per year ($p < 0.05$). 94.57% of the pixels presented an increasing trend in ET, among which 95% of these pixels passed the significance test (Fig. 3f).

3.1.2. Spatial-temporal conversion and variations of each land-use type

Fig. 4a presents the distribution, composition, and spatial dynamics of land-use types in the study area. Despite the notable discrepancies in land-use types in 2000 and 2015, their distribution was rather similar. Taking the year 2015 as an example, the main landscapes include grassland (60,326.92 km^2, occupying 41.14% of the study area), barren land (52,664.20 km^2, occupying 35.92%), and cultivated land (24,246.56 km^2, occupying 16.54%). The remaining three land use types (including water bodies, construction land, and woodland) accounted for 6.40% of the study area. We observed that increased

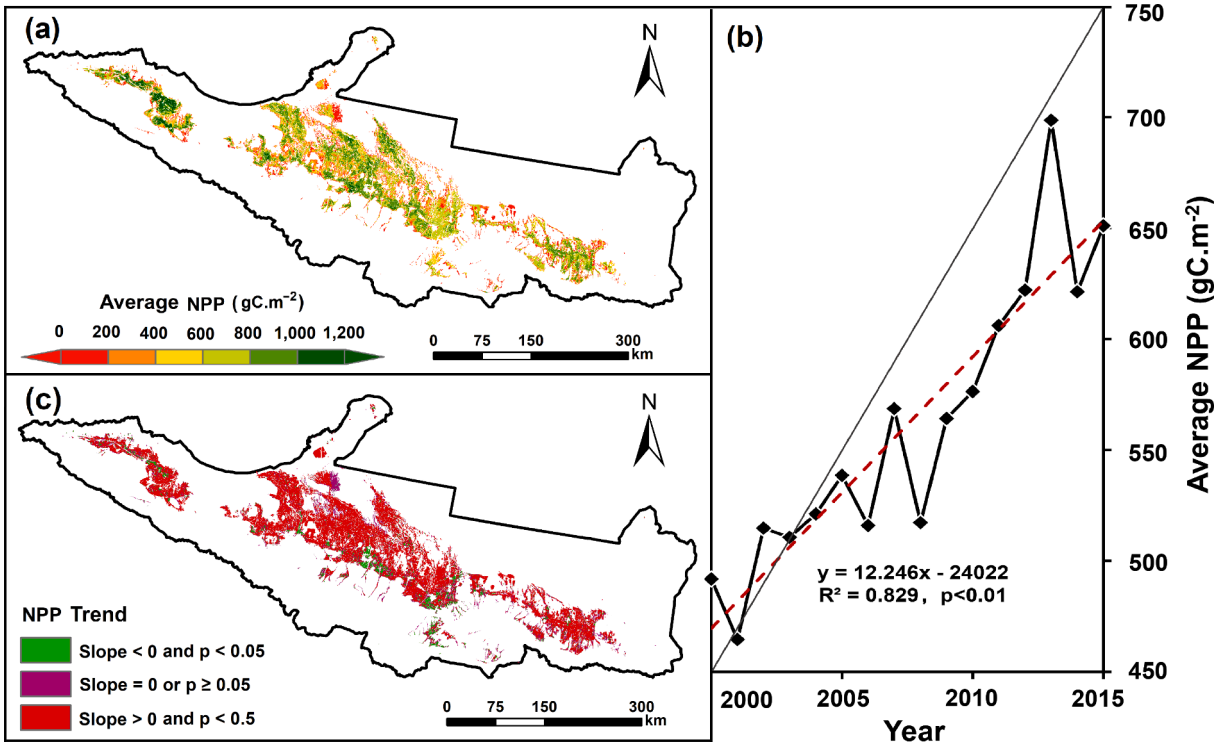

Fig. 2. (a) Spatial distribution of average annual NPP in the farmland ecosystem; (b) Inter-annual variations of NPP from 2000 to 2015; (c) Pixel-wise spatial–temporal trend of annual NPP.

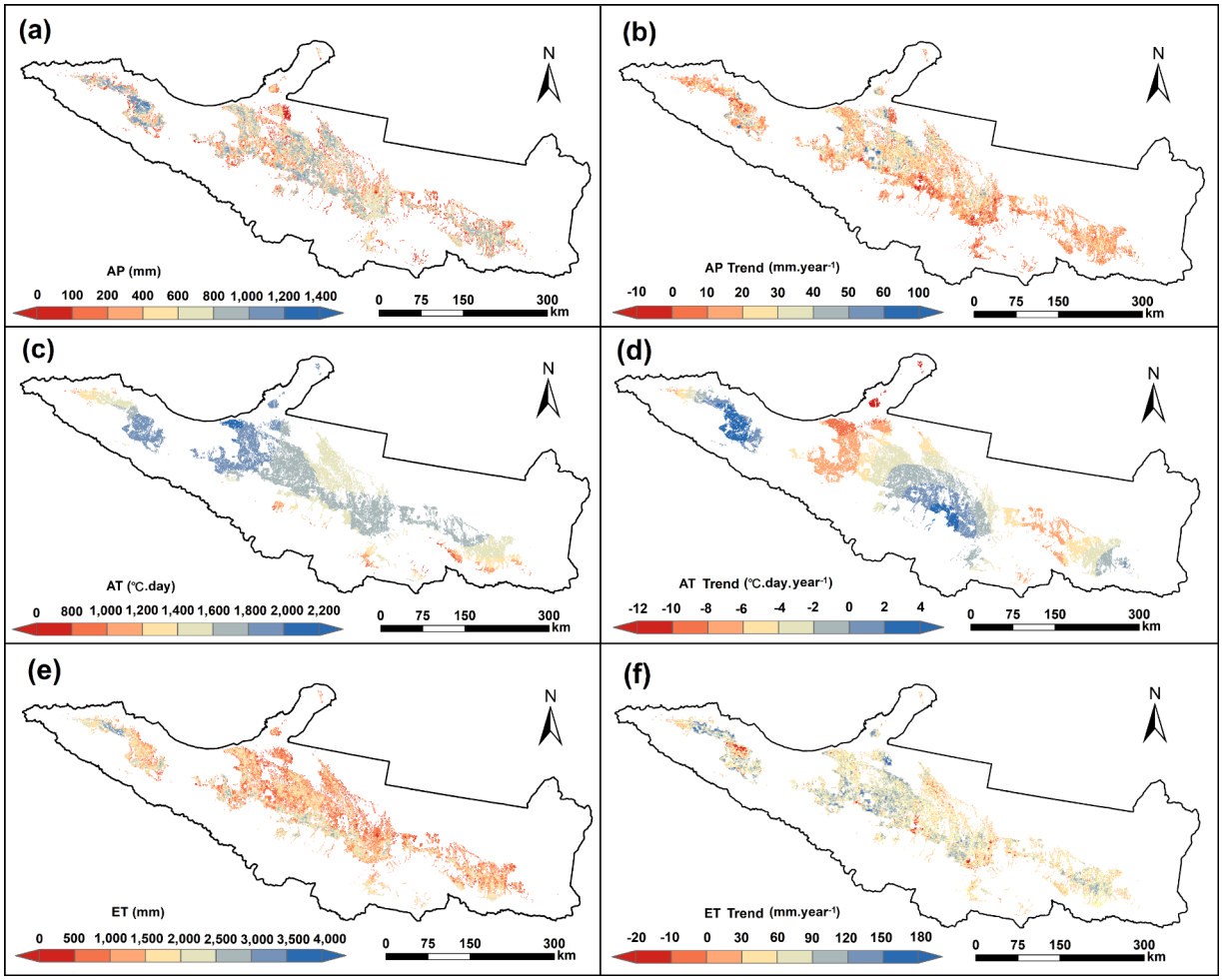

Fig. 3. Spatial distribution and spatial–temporal trend of AP (a and b), AT (c and d), and ET (e and f) in the farmland ecosystem during 2000–2015.

cultivated land (3683.55 km^2) is larger than the decreased cultivated land (889.44 km^2).

The statistical results showed that the land use types had undergone tremendous changes. The scales of conversion among various landscape patterns in 3 sub-districts were notably different (Fig. 4b, 4c, and 4d). We noted two phenomena. First, cultivated land encroached a large amount of grassland (3,187.66 km^2), accounting for 86.54% of the increased cultivated land. Second, cultivated land has decreased by 889.44 km^2, of which 604.79 km^2 was converted into construction land. Lost cultivated land were found concentrated around the urban fabrics.

3.1.3. Dynamics of soil salinization in FES at pixel scale

The spatial distribution of soil salinization in the farmland ecosystem is shown in Fig. 5. Taking the year 2015 as an example, the results indicated that none salinization (covering an area of 16,460.96 km^2) was dominant in the study area, occupying 67.89% of the farmland system. What worries us is that>30% of farmland was threatened by soil salinization (i.e., mild salinization at 27.15%, moderate salinization at 4.95%, and severe salinization at 0.01%). We found that cultivated land with none salinization decreased by 485.73 km^2, most of which was converted to other land use types (472.79 km^2), a small amount was converted to mild (11.37 km^2) and moderate salinization (1.57 km^2). Increased none salinized cultivated lands cover 1,546.82 km^2. 53.35 km^2 of mild soil salinization and 27.32 km^2 of moderate salinization were transformed into none salinization. Despite that the net increase in none salinization was 1061.09 km^2, a large amount of high-quality cultivated land was converted to other landscapes, mainly including construction land and grassland.

3.1.4. Advances in agricultural management practices

We explored the evolution of 3 typical AMPs (i.e., mulching filming rate, drip irrigation rate, and fertilizer application) during the study period. Firstly, the mulching filming rate of increased from 28.29% in 2000 to 53.05% in 2015 (Table 2). Secondly, changes in soil moisture and distribution caused by irrigation methods have an important impact on vegetable production capacity. As of 2015, the area of drip irrigation farmland accounted for 46.13% of the total farmland, while it was only 28.74% in 2000. Thirdly, reducing the application of chemical fertilizer and increasing fertilizer efficiency has a positive contribution to the NPP dynamics. The fertilizer application decreased from 295.83 kg/hm^2 in 2000 to 206.59 kg/hm^2 in 2015.

3.2. Impacts of soil salinization on NPP in FES

From the perspective of pixel scale, the NPP value of non-salinized farmland (631.06 $gC.m^{-2}$) is higher than the average value of farmland ecosystem (561.72 $gC.m^{-2}$) (Table 3). The NPP of the salinized farmland is lower than the average value of the farmland ecosystem, and the severer the salinization, the lower the NPP (437.62 $gC.m^{-2}$ in mild salinization, 352.57 $gC.m^{-2}$ in moderate salinization, 316.36 $gC.m^{-2}$ in severe salinization). We further calculated the anomaly of NPP on each type of salinized cultivated land. Compared with the entire study area, the NPP of non-salinized cultivated land increased by 1.14 Tg C per year on average, mild salinized land decreased by 0.82 Tg C per year,

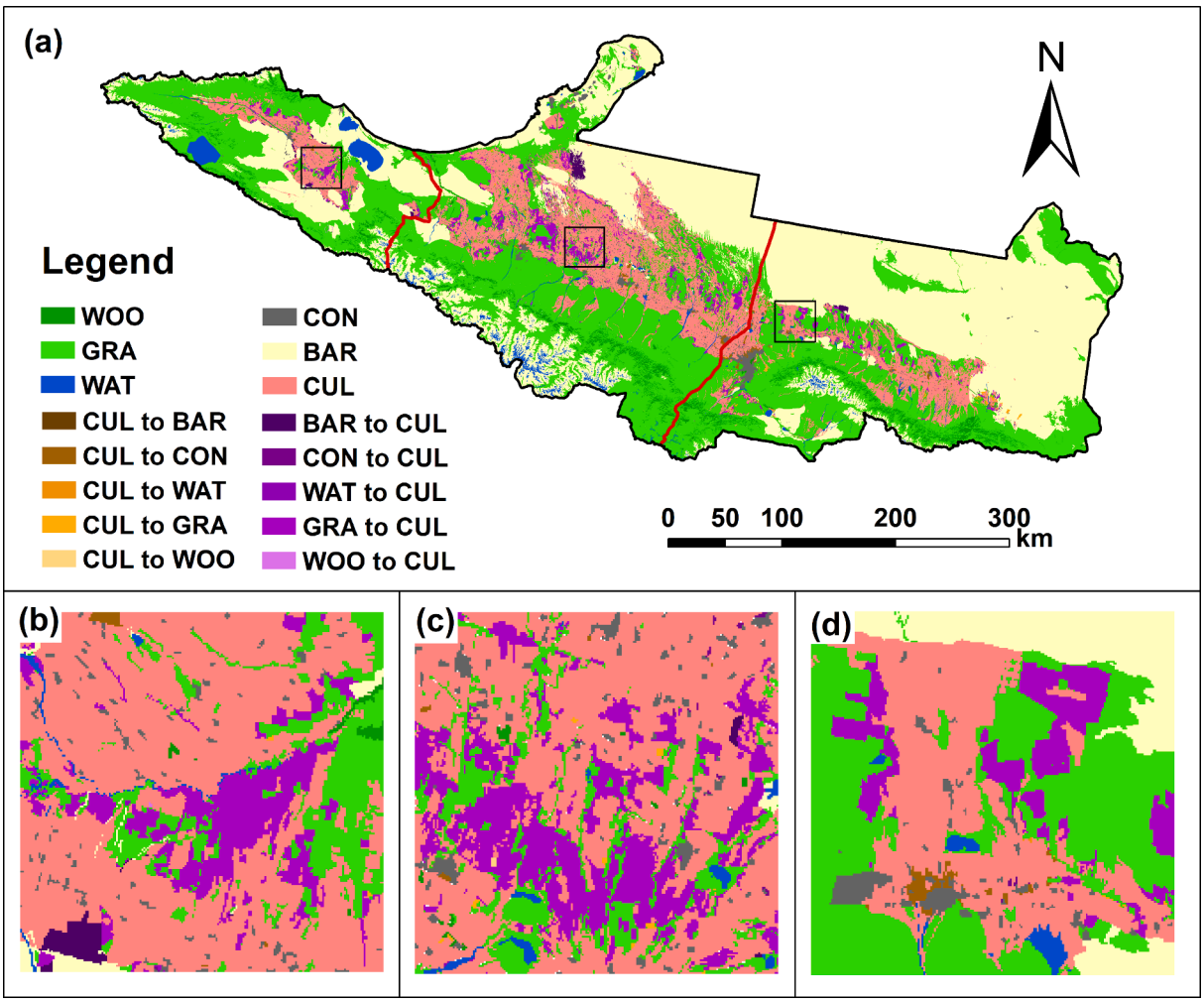

Fig. 4. (a) Spatial-temporal conversion of land-use types in the study area from 2000 to 2015, typical display of land-use dynamics in the west (b), central (c), and east sub-district (d). Note: WOO: woodland; GRA: grassland; WAT: water body; CON: construction land; BAR: barren land; CUL: cultivated land.

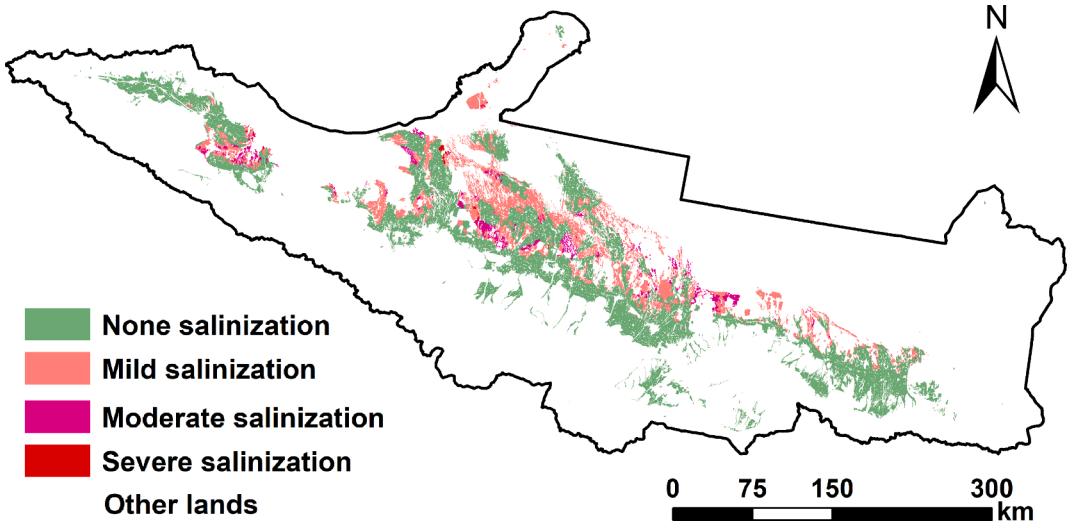

Fig. 5. Distribution of soil salinization in the investigated farmland ecosystem.

moderate salinized land decreased by 0.25 Tg C per year, and severe salinized land decreased 0.0004 Tg C per year. The above results indicate that the higher the degree of soil salinization, the stronger the inhibitory effect on NPP.

3.3. Contribution of climate, AMPs, urbanization, and soil to NPP dynamics in FES

Our results suggest that the total NPP of FES increased by 3.86 Tg C

Table 2
Temporal evolution of typical AMPs during 2000–2015 in FES.

Year	Mulching filming rate (%)	Drip irrigation rate (%)	Fertilizer application(kg/hm^2)
2000	28.29	28.74	295.83
2005	31.02	30.13	250.03
2010	43.46	35.40	217.66
2015	53.05	46.13	206.59

from 2000 to 2015. We further explored the contribution of climate change, AMPs, urbanization, soil salinization, and residual factors to the NPP dynamics. The results revealed that climate factors contribute to an increase in NPP by 4.01 Tg C, where AP contributed 0.68 Tg C, AT contributed 0.96 Tg C, and ET contributed 2.37 Tg C. Compared with the initial NPP in 2000 (491.83 gC.m^{-2}), these climatic factors have distinctly promoted the increase of NPP. Results from correlation analysis and linear regression model show that NPP and AP are significantly positively correlated in FES ($R^2 = 0.442$, $p < 0.05$). In addition, there is a significant positive correlation between NPP and AT ($R^2 = 0.671$, $p < 0.01$). The correlation between NPP and ET is also found statistically positive ($R^2 = 0.901$, $p < 0.01$).

Advances in AMPs contributed positively to NPP dynamics (+0.98 Tg C). Film mulching contributed 0.41 Tg C, suggesting a high promoting effect on the stability of surface soil aggregates. During the investigated period in the study area, 304.79 km^2 of cultivated land was occupied by urbanization. Urbanization has reduced the total NPP by 0.16 Tg C. However, this amount accounts for only a small percentage (2.67%) of the NPP anomaly, which is inconsistent with the results from existing studies. We discussed this issue in a detailed manner in the discussion section.

Soil salinization led to a decrease of 1.07 Tg C in NPP. Compared with the average NPP of none salinization (631.06 gC.m^{-2}), soil salinization largely weakened the growth of NPP. Our results revealed that the severer the soil salinization, the stronger the inhibitory effect on NPP. Mild salinization, which weakened NPP by 193.44 gC.m^{-2} with an area of 6,583.21 km^2, resulted in a decrease of 0.82 Tg C in the total NPP. Moderate salinization weakened NPP by 278.49 gC.m^{-2} with an area of 1200.83 km^2, resulting in a decrease of 0.25 Tg C in the total NPP. Severe salinization has the strongest inhibitory effect on NPP per unit area (314.70 gC.m^{-2}). However, due to the small spatial coverage of severe salinization (only 1.56 km^2), its impact on the total NPP is minimal (0.0004 Tg C). The statistical results reveal that the residual factors (e.g., crop species, planting system, etc.) promote an increase in the total NPP by 0.10 Tg C.

4. Discussion

4.1. Spatial-temporal dynamics of NPP in arid FES

Efforts have been made to explore the spatial–temporal dynamics of NPP at the scale of city (Luo et al., 2018; Nuarsa et al., 2018), region (Zhang et al., 2016; Pan et al., 2021), country (Chen and Zeng 2016; He et al., 2017), and global (Field et al., 1995; Song et al., 2019) (Table 4). It has been widely acknowledged that land use types differ in structure, function, and ecological carrying capacity. Given the relationship among land resources, biological environment, and biological populations, FES can be categorized as a semi-natural and semi-artificial ecosystem. It not only plays a fundamental role in food production but also assumes indirect functions such as ecological services, environmental regulation, and cultural services. Therefore, we aim to simulate and analyze the NPP spatial–temporal dynamics specifically in FES, using the VPM model by taking the northern slope of the Tianshan Mountains as a study case.

NPP monitoring in farmland ecosystems in the world is extremely important, especially in arid and semiarid farmland ecosystems, given its vulnerability to climate change and human perturbation (Alton 2020; Chen et al., 2013; Li et al., 2020; Tian et al., 2016) (Table 5). For example, Zhang and Ren (2017) stated that the dryland's response to warming was weak, while its cropland was sensitive to the CO2 fertilization effect in central Asia. Pan et al. (2021) pointed out that land use change had less effect on total NPP than climate change in global drylands. Especially, the world is on the verge of the worst food crisis in at least 50 years (Asiedu et al., 2020). Weiss et al. (2020) presented a summary of applications in remote sensing technology that targets agricultural development, e.g., agricultural applications include crop breeding, agricultural land use monitoring, crop yield forecasting, as well as ecosystem services in relation to soil and water resources or biodiversity loss.

Previous studies have been conducted using multi-source remote sensing images and ecological models to estimate the NPP on the northern slope of the Tianshan Mountains (Table 6). Zhang and P. A. N. (2010) used Production Efficiency Model for Net Primary Productivity (NPP-PEM) to estimate the spatial distribution of NPP and its seasonal changes in ecological transects. Their results show that the average NPP of the mountain-oasis-desert ecological transect is 161.06 gC·m^{-2}. Han et al. (2014) used the Biome-BGC model to simulate the changing trend of NPP in the forest ecosystem on the northern slope of the Tianshan Mountains from 1959 to 2009. A study by Gao et al. (2018) proved that NPP differs in land cover types using the CASA model. Their results reveal that the NPP for woodland, cultivated land, grassland, and barren

Table 3
Temporal heterogeneity of NPP with different degrees of soil salinization in FES.

Year	None		Mild		Moderate		Severe		FES	
	NPP gC.m^{-2}	△NPP Tg C	NPP gC.m^{-2}	△NPP Tg C	NPP gC.m^{-2}	△NPP Tg C	NPP gC.m^{-2}	△NPP Tg C	NPP gC.m^{-2}	Total Tg C
2000	563.60	1.18	356.82	−0.89	279.55	−0.25	216.47	−0.0004	491.83	11.93
2001	540.30	1.25	324.41	−0.92	249.57	−0.26	190.69	−0.0004	464.55	11.26
2002	591.34	1.26	374.77	−0.92	303.47	−0.25	248.57	−0.0004	514.73	12.48
2003	589.97	1.31	363.09	−0.97	273.64	−0.28	209.90	−0.0005	510.66	12.38
2004	599.54	1.29	378.87	−0.94	286.83	−0.28	217.37	−0.0005	521.18	12.64
2005	620.41	1.35	392.1	−0.96	282.42	−0.31	200.82	−0.0005	538.53	13.06
2006	597.72	1.35	372.26	−0.95	274.00	−0.29	205.51	−0.0005	515.97	12.51
2007	662.13	1.54	401.43	−1.10	294.48	−0.33	241.78	−0.0005	568.64	13.79
2008	578.48	1.01	414.81	−0.67	323.68	−0.23	288.62	−0.0004	517.29	12.54
2009	648.15	1.38	414.88	−0.98	313.12	−0.30	272.98	−0.0005	564.13	13.68
2010	646.27	1.15	454.33	−0.80	363.05	−0.26	319.62	−0.0004	576.30	13.97
2011	664.96	0.97	505.41	−0.66	416.58	−0.23	361.46	−0.0004	606.07	14.70
2012	673.47	0.85	535.23	−0.57	451.57	−0.20	445.35	−0.0003	622.05	15.08
2013	755.04	0.93	599.12	−0.65	518.01	−0.22	430.08	−0.0004	698.59	16.94
2014	655.68	0.57	557.28	−0.42	517.73	−0.12	467.26	−0.0002	621.26	15.06
2015	704.14	0.87	551.19	−0.66	498.94	−0.18	445.35	−0.0003	651.07	15.79
Mean	631.06	1.14	437.62	−0.82	352.57	−0.25	316.36	−0.0004	561.72	

Table 4
Comparison of findings of selected representative studies.

Study Area	Associated Object	Model/Methods	Findings	Sources
Global	Terrestrial ecosystem	CASA model	NPP models that include richer suites of controlling parameters should be more sensitive to conditions that disrupt the broad correlations.	Field et al. 1995
Central Asia	Dryland ecosystems	Arid Ecosystem Model	The dryland's response to warming is weak, while its cropland is sensitive to the CO2 fertilization effect.	Zhang and Ren 2017
China	Farmland	CASA model	Rapid urban expansion from 1992 to 2015 causes stress to China's food security.	He et al. 2017
West African	Woodlands, farmlands	Proposed technical framework	Vegetation acts as a carbon sink and provides ecosystem services for local people	Brandt et al. 2018
Lingwu City, China	Farmland	Linear fitting, time series fusion, spatial–temporal fusion model	The time series fusion model and spatial–temporal fusion model are suitable for the dynamic monitoring of farmland productivity.	Luo et al. 2018
Global	Terrestrial ecosystem	Global P-model simulations	Drought impacts on terrestrial primary production are underestimated	Stocker et al. 2019
Xinjiang, China	Vegetation	CASA model	Climate change promotes an increase in NPP, while human activities reduce NPP.	Jiang et al. 2020
Drylands	Terrestrial ecosystem	Ridge-regression evaluation method	Land use dynamics have less effect on total NPP in drylands than climate change.	Pan et al. 2021

land were 534. 47 gC.m^{-2}, 333. 47 gC.m^{-2}, 174. 20 gC.m^{-2} and 124. 18 gC.m^{-2}, respectively. Using MODIS series data, Yin et al. (2020) found that the NPP showed an overall increasing trend (from 14.74 Tg C to 19.53 Tg C) on the northern slope of Tianshan Mountains from 2004 to 2015.

Our results show that the total NPP of FES has increased by 3.86 Tg C from 2000 to 2015. The changing trend of NPP is consistent with the previous studies, and the anomaly of NPP is larger than that of them. The discrepancy of impervious surface distribution between our studies and previous studies can be attributed in part to (1) the different calculation principles of models; (2) different remote sensing images that were used in land cover classification. In our research, we used all Landsat images that are available during the investigated period, which reduces the number of non-data pixels due to cloud cover and shadows. We also incorporated some economic forests (e.g., vineyards, fruit trees, etc.) and short-term idle arable land into FES.

4.2. Combined impacts of climate change, soil salinization, urbanization, and AMPs on farmlands' NPP

The conceptual framework designed in this study and the documented influence of "climate change, urbanization, soil salinization and AMPs" on NPP provide new insights on the sustainable development of agriculture in arid areas. In this study, we proved that climate change and AMPs have a positive impact on farmland NPP, whereas soil salinization and urbanization have a negative impact on it. By analyzing the influence of each variable on vegetation productivity, the joint influence mechanism was revealed. The results show that climate change has led to an increase in farmland NPP by 4.10 Tg C (0.68 Tg C from AP, 0.96 Tg C from AT, and 2.07 Tg C from ET) from 2000 to 2015 in our study area. We believe that climate change is one of the main reasons for the growth of NPP, which is consistent with previous conclusions (Chen et al., 2013; Ji et al., 2019; Rudgers et al., 2018; Yao et al., 2018). Most of these studies adopted correlation analysis to explore the relationship between impact factors and NPP. Their main contribution is to investigate whether these factors have significant or insignificant impacts on NPP. However, such an approach fails to measure how much these factors contribute to the anomaly of NPP. Our study reveals the specific contribution of three typical climate factors (i.e., AP, AT, and ET) to the NPP anomaly.

We also quantified the impact of soil salinization on NPP in FES, an issue that few studies have investigated. It is widely acknowledged that soil is one of the most basic environments for vegetation growth and a very important eco-chemical index (Bless et al., 2018; Funakawa et al., 2000; Smith et al., 2016). Soil conditions directly affect the growth state of vegetation (Gebremeskel et al., 2018; Rath and Rousk 2015). As a comprehensive index to characterize soil quality, the role of soil salinization on NPP has been thoroughly explored. Our results show that soil salinization greatly weakens the climate-driven NPP growth (-1.07 Tg C), with varying severity of soil salinization leading to varying NPP anomalies. Specifically, NPP in mildly salinized land decreased by 0.82 Tg C per year, NPP in moderately salinized land decreased by 0.25 Tg C per year, and NPP in severely salinized land decreased by 0.0004 Tg C per year (due to the small coverage of severely salinized areas). Our study reveals the role of soil improvement in responding to the food crisis, providing numerous valuable references to improve the vegetation productivity in FES: (1) avoiding excessive use of chemical fertilizers to improve soil environment; (2) converting severe salinized cultivated land into forest land to enhance the carbon sequestration capacity of FES; (3) establishing warning lines near cities to prevent more non-salinized farmland from being encroached on.

Many pieces of evidence have confirmed the negative impact of urbanization on NPP at both global scale and varying regional scales (Buyantuyev and Wu 2009; d'Amour et al., 2017; Dong et al., 2015; He et al., 2017; Li et al., 2016; Trinder and Liu 2020). Liu et al., 2019b suggested that the urbanization-induced decrease in NPP offset 30% of the climate-driven increase (73.6 Tg C year − 1) between 2000 and 2010 in the world. Zhong et al. (2019) showed that 38.0% and 28.0% decreasing trends of EVI and GPP occurred in *peri*-urban and rural areas due to land use and land cover conversion during 2000–2016 in Shanghai, China. In comparison, results from our study confirmed that the weakening effect of urbanization on the NPP in FES (-0.16 Tg C, occupying 2.67% of NPP anomaly) is lower than that of existing studies. This can be presumably explained by two reasons: (1) the degree/speed of urbanization in arid areas is considerably lower than that in non-arid areas; (2) urbanization invades not only cultivated land but also other land cover types (e.g., woodland and grassland), and this study only considers the impact of impervious surface expansion on the farmland ecosystem. Therefore, we encourage more efforts to be made to distinguish the difference between arid regions and other regions when evaluating the impacts of urbanization on NPP.

Our findings further support the argument that advances in AMPs contribute positively (+0.98 Tg C) to NPP dynamics, consistent with many existing studies. Existing efforts paid more attention to the changes in tillage patterns (including no-tillage, reduced-tillage, and direct drilling), while in some areas, tillage patterns have not changed for many years. Therefore, we attached more emphasis on selecting appropriate AMPs (e.g., mulching filming, drip irrigation, and fertilizer application) at the regional scale. We believe the reduction in coverage of plastic film is beneficial to the vegetable production capacity. The drip irrigation that gradually replaces flood irrigation at a large scale is also beneficial, as it improves the efficiency of agricultural water use in

Table 5
Summary of selected representative related studies.

Study area	Objects	Dependent variables	Independent variables	Findings	Limitations	Sources
Qinghai-Tibetan Plateau	Forest and grassland	NPP	Precipitation, temperature, and LUCC	The warmer and wetter climate has increased NPP and soil respiration.	Ignore the soil indicators	Chen et al. 2013
Amazonia	Forest	NPP	Drought	Drought suppresses Amazon-wide photosynthesis in 2010 by 0.38 pg C.	Just focus on drought	Doughty et al. 2015
West African Sahel	Herbaceous and woody plant	NDVI and VOD	Precipitation	VOD captures variations of woody plant foliage biomass better than NDVI.	Single indicator	Tian et al. 2016
Xinjiang, China	Grassland	NPP	Grazing	Grazing reduces the NPP of grassland.	Single indicator	Huang et al. 2018
China	Vegetation	NPP	Severe drought events	Severe drought events induce decreases in NPP.	Single indicator	Li et al. 2020
Global	Forest and grassland	GPP and NPP	Precipitation and temperature	Global productivity is dominated by tropical/needle leaf forest & C3 grass/crops.	Just focus on climate change	Alton 2020
South Mediterra-nean	Grassland	NPP	Precipitation and temperature	NPP increases along with the decrease in precipitation and temperature.	Just focus on climate change	Ghiloufi and Chaieb 2021
NSTM	Farmland	NPP	Urbanization, climate, APMs, soil salinization	Comprehensive and quantitative assessment of the impact of climate change, urbanization, soil salinization and AMPs on farmland NPP.	/	This study

Note: GPP: Gross Primary Productivity; VOD: vegetation optical depth; NDVI: Normalized Difference Vegetation Index; NSTM: the Northern Slope of Tianshan Mountains.

Table 6
Comparisons of simulated NPP in this study and existing studies.

Model	Area	Period	Object	Mean NPP	Advantage	Disadvantage	Reference
NPP-PEM	NSTM	2002	region	161.06	Strong applicability in arid ecosystems	Poor spatial analyzability, unclear mechanism	Zhang and P. A. N. (2010)
Biome-BGC	NSTM	1959–2009	woodland	547.97	More sensitive to climate change	Lack of verification	Han et al. (2014)
CASA	NSTM	2015	region	173.34	Requires fewer parameters	Complicated calculation process	Gao et al. (2018)
MOD17A3H	NSTM	2004–2015	region	144.71	Easy to get	Accuracy cannot be guaranteed	Yin et al. (2020)
VPM	NSTM	2000–2015	FES	561.72	Simple input parameters, high precision, fast calculation	Actual NPP may be overestimated	this study

arid areas and potentially increases production capacity by providing reasonable irrigation for different crops. The reduction of fertilizer application enhances the vegetable production capacity (+0.12 Tg C) by reducing the cumulative mineralization amount and cumulative mineralization rate of SOC. We have to point out that this also includes the contribution of organic fertilizer. The statistical results indicate that the increase in mulching filming rate, the increase of drip irrigation area, and the reduction of fertilizer application promoted the NPP in FES.

5. Conclusion

This study aims to assess the joint impact of "climate-urbanization-soil-AMPs" on the NPP of the farmland ecosystems (FES) under the background of the global food crisis. The inter-annual variations and trends of NPP indicate that the vegetation productivity in FES showed a significant increasing trend from 2000 to 2015. We further quantified the positive and negative effects of these factors on NPP. The quantitative analysis shows that climate warming (increased accumulated temperature), humidification (increased precipitation), and advances in AMPs have promoted the NPP. In contrast, soil salinization and urbanization have weakened the growth of NPP. The results also suggest that soil salinization is more detrimental to NPP than urbanization.

Our study marks a pioneering attempt that reveals the joint impact and individual impacts of "climate-urbanization-soil-AMPs" on the NPP in arid FES, taking advantage of (1) Landsat and MODIS images, (2) climate datasets, (3) the vegetation photosynthesis model (VPM), (4) measured soil data, and (5) a novel conceptual evaluating framework. Our results are expected to benefit farmland users and land planners in better managing agricultural land. Although the results of this study are specific to the farmland ecosystem on the northern slope of the Tianshan Mountains, the conceptual and methodological design in this study can be adapted to other regions through changes, deletions or additions to the indicators. With the development of remote sensing technology, the indicators involved in this study can be quantitatively retrieved through remote sensing images (e.g., soil salinization), thus avoiding time-consuming and laborious field sampling work. Future efforts are encouraged to further optimize the proposed evaluating framework and adapt it to explore the changing mechanism of vegetation productivity in larger geographical regions.

Funding information

This work is supported by the National Key Research and Development Program of China under Grant 2018YFB0505401, the Research Project from the Ministry of Natural Resources of China under Grant 4201 240100123, the National Natural Science Foundation of China under Grants 41771452, 41771454, and 41890820, the Natural Science Fund of Hubei Province in China under Grant 2018CFA007.

Declaration of Competing Interest

The authors declare that they have no known competing financial interests or personal relationships that could have appeared to influence the work reported in this paper.

Acknowledgments

We would like to extend sincere gratitude to the academic editor and reviewers for their constructive comments which greatly helped us to improve the quality of this manuscript.

Appendix A. Supplementary data

Supplementary data to this article can be found online at https://doi.org/10.1016/j.geoderma.2022.115712.

References

Alton, P.B., 2020. Representativeness of global climate and vegetation by carbon-monitoring networks; implications for estimates of gross and net primary productivity at biome and global levels. Agric. For. Meteorol. 290, 108017. https://doi.org/10.1016/j.agrformet.2020.108017.

Asiedu, E., Sadekla, S.S., Bokpin, G.A., 2020. Aid to Africa's agriculture towards building physical capital: Empirical evidence and implications for post-COVID-19 food insecurity. World development perspectives 20, 100269.

Bless, A.E., Colin, F., Crabit, A., Devaux, N., Philippon, O., Follain, S., 2018. Landscape evolution and agricultural land salinization in coastal area: A conceptual model. Sci. Total Environ. 625, 647–656.

Brandt, M., Rasmussen, K., Hiernaux, P., Herrmann, S., Tucker, C.J., Tong, X., Tian, F., Mertz, O., Kergoat, L., Mbow, C., David, J.L., Melocik, K.A., Dendoncker, M., Vincke, C., Fensholt, R., 2018. Reduction of tree cover in West African woodlands and promotion in semiarid farmlands. Nat. Geosci. 11 (5), 328–333.

Buyantuyev, A., Wu, J., 2009. Urbanization alters spatiotemporal patterns of ecosystem primary production: A case study of the Phoenix metropolitan region, USA. J. Arid Environ. 73 (4-5), 512–520.

Chen, H., Zhu, Q., Peng, C., Wu, N., Wang, Y., Fang, X., Gao, Y., Zhu, D., Yang, G., Tian, J., Kang, X., Piao, S., Ouyang, H., Xiang, W., Luo, Z., Jiang, H., Song, X., Zhang, Y., Yu, G., Zhao, X., Gong, P., Yao, T., Wu, J., 2013. The impacts of climate change and human activities on biogeochemical cycles on the Qinghai-Tibetan Plateau. Glob. Change Biol. 19 (10), 2940–2955.

Chen, J., Liu, J., Luo, X., 2020. Improving the Penman-Monteith evapotranspiration model based on the coupling principle of carbon and water fluxes. J. Atmos. Sci. 43, 59–75.

Chen, X., Zeng, Y., 2016. Spatial and temporal variability of the net primary production (NPP) and its relationship with climate factors in subtropical mountainous and hilly regions of China: A case study in Hunan province. Acta Geographica Sinica 71, 35–48.

Bren d'Amour, C., Reitsma, F., Baiocchi, G., Barthel, S., Güneralp, B., Erb, K.-H., Haberl, H., Creutzig, F., Seto, K.C., 2017. Future urban land expansion and implications for global croplands. PNAS 114 (34), 8939–8944.

Daliakopoulos, I.N., Tsanis, I.K., Koutroulis, A., Kourgialas, N.N., Varouchakis, A.E., Karatzas, G.P., Ritsema, C.J., 2016. The threat of soil salinity: A European scale review. Sci. Total Environ. 573, 727–739.

Dehaan, R.L., Taylor, G.R., 2002. Field-derived spectra of salinized soils and vegetation as indicators of irrigation-induced soil salinization. Remote Sens. Environ. 80 (3), 406–417.

Dong, G., Bai, J., Yang, S., Wu, L., Cai, M., Zhang, Y., Luo, Y.a., Wang, Z., 2015. The impact of land use and land cover change on net primary productivity on China's Sanjiang Plain. Environ. Earth Sci. 74 (4), 2907–2917.

Doughty, C.E., Metcalfe, D.B., Girardin, C.A.J., Amézquita, F.F., Cabrera, D.G., Huasco, W.H., Silva-Espejo, J.E., Araujo-Murakami, A., da Costa, M.C., Rocha, W., Feldpausch, T.R., Mendoza, A.L.M., da Costa, A.C.L., Meir, P., Phillips, O.L., Malhi, Y., 2015. Drought impact on forest carbon dynamics and fluxes in Amazonia. Nature 519 (7541), 78–82.

FAO, I., UNICEF, WFP and WHO (2020). *The State of Food Security and Nutrition in the World 2020. Transforming food systems for affordable healthy diets*. In FAO (Ed.). Rome.

Farzamian, M., Paz, M.C., Paz, A.M., Castanheira, N.L., Gonçalves, M.C., Monteiro Santos, F.A., Triantafilis, J., 2019. Mapping soil salinity using electromagnetic conductivity imaging—A comparison of regional and location-specific calibrations. Land Degrad. Dev. 30 (12), 1393–1406.

Field, C.B., Randerson, J.T., Malmström, C.M., 1995. Global net primary production - combining ecology and remote-sensing. Remote Sens. Environ. 51 (1), 74–88.

Funakawa, S., Suzuki, R., Karbozova, E., Kosaki, T., Ishida, N., 2000. Salt-affected soils under rice-based irrigation agriculture in southern Kazakhstan. Geoderma 97 (1-2), 61–85.

Gao, J., Yin, X., Wang, C., Zhang, Y., 2018. Spatial - temporal Distribution of NPP and Its Climatic Driving Factors in the Northern Slope of Tianshan Mountain. Xinjiang Agricultural Sciences 55, 352–361.

Gebremeskel, G., Gebremicael, T.G., Hagos, H., Gebremedhin, T., Kifle, M., 2018. Farmers' perception towards the challenges and determinant factors in the adoption of drip irrigation in the semiarid areas of Tigray, Ethiopia. Sustain. Water Resour. Manag. 4 (3), 527–537.

Ghiloufi, W., Chaieb, M., 2021. Environmental factors controlling vegetation attributes, soil nutrients and hydrolases in South Mediterranean arid grasslands. Ecol. Eng. 161, 106155. https://doi.org/10.1016/j.ecoleng.2021.106155.

Gregg, J.W., Jones, C.G., Dawson, T.E., 2003. Urbanization effects on tree growth in the vicinity of New York City. Nature 424 (6945), 183–187.

Han, Q., Luo, G., Li, C., Ye, H., Feng, Y., 2014. Simulation of Carbon Trend in Forest Ecosystem in Northern Slope of the Tianshan Mountains Based on Biome-BGC Model. Arid Zone Res. 31, 375–382.

He, C., Liu, Z., Xu, M., Ma, Q., Dou, Y., 2017. Urban expansion brought stress to food security in China: Evidence from decreased cropland net primary productivity. Sci. Total Environ. 576, 660–670.

Huang, M., Piao, S., Ciais, P., Peñuelas, J., Wang, X., Keenan, T.F., Peng, S., Berry, J.A., Wang, K., Mao, J., Alkama, R., Cescatti, A., Cuntz, M., De Deurwaerder, H., Gao, M., He, Y., Liu, Y., Luo, Y., Myneni, R.B., Niu, S., Shi, X., Yuan, W., Verbeeck, H., Wang, T., Wu, J., Janssens, I.A., 2019. Air temperature optima of vegetation productivity across global biomes. Nat. Ecol. Evol. 3 (5), 772–779.

Huang, X., Luo, G., Ye, F., Han, Q., 2018. Effects of grazing on net primary productivity, evapotranspiration and water use efficiency in the grasslands of Xinjiang, China. J. Arid Land 10 (4), 588–600.

Islam, M.A., Hoque, M.A., Ahmed, K.M., Butler, A.P., 2019. Impact of Climate Change and Land Use on Groundwater Salinization in Southern Bangladesh-Implications for Other Asian Deltas. Environ Manage 64 (5), 640–649.

Ji, P., Gao, M., Yang, X., 2019. Analysis of NPP driving force in an arid region of Northwest China: A case study in Yili Valley and parts of Tianshan Mountains, Xinjiang, China. Acta Ecologica Sinica 39, 2995–3006.

Jiang, L., Jiapaer, G., Bao, A., Kurban, A., Guo, H., Zheng, G., De Maeyer, P., 2019. Monitoring the long-term desertification process and assessing the relative roles of its drivers in Central Asia. Ecol. Ind. 104, 195–208.

Jiang, Y., Guo, J., Peng, Q., Guan, Y., Zhang, Y., Zhang, R., 2020. The effects of climate factors and human activities on net primary productivity in Xinjiang. Int. J. Biometeorol. 64 (5), 765–777.

Jones, M.O., Running, S.W., Kimball, J.S., Robinson, N.P., Allred, B.W., 2020. Terrestrial primary productivity indicators for inclusion in the National Climate Indicators System. Clim. Change 163 (4), 1855–1868.

Kansiime, M.K., Tambo, J.A., Mugambi, I., Bundi, M., Kara, A., Owuor, C., 2021. COVID-19 implications on household income and food security in Kenya and Uganda: Findings from a rapid assessment. World Dev. 137, 105199. https://doi.org/10.1016/j.worlddev.2020.105199.

Khongnawang, T., Zare, E., Srihabun, P., Triantafilis, J., 2020. Comparing electromagnetic induction instruments to map soil salinity in two-dimensional cross-sections along the Kham-rean Canal using EM inversion software. Geoderma 377, 114611. https://doi.org/10.1016/j.geoderma.2020.114611.

Kong, C., Xu, K., Yue, Y., 2021. Assessment impacts of climate variability and LULC change on net primary productivity in the process of rapid urbanization: a case study in Jianghan Plain of China. Geocarto International 36 (5), 499–519.

Le Noë, J., Billen, G., Mary, B., Garnier, J., 2019. Drivers of long-term carbon dynamics in cropland: A bio-political history (France, 1852–2014). Environ. Sci. Policy 93, 53–65.

Li, G., Zhang, H., Chen, S., Qiu, J., Wang, X., 2016. Assessing the impact of urban development on net primary productivity during 2000–2010 in Taihu Basin. Environ. Earth Sci. 75, 1266.

Li, J., Wang, Z., Lai, C., 2020. Severe drought events inducing large decrease of net primary productivity in mainland China during 1982–2015. Sci. Total Environ. 703, 135541. https://doi.org/10.1016/j.scitotenv.2019.135541.

Liu, H., Mi, Z., Lin, L.i., Wang, Y., Zhang, Z., Zhang, F., Wang, H., Liu, L., Zhu, B., Cao, G., Zhao, X., Sanders, N.J., Classen, A.T., Reich, P.B., He, J.-S., 2018. Shifting plant species composition in response to climate change stabilizes grassland primary production. PNAS 115 (16), 4051–4056.

Liu, X., Pei, F., Wen, Y., Li, X., Wang, S., Wu, C., Cai, Y., Wu, J., Chen, J., Feng, K., Liu, J., Hubacek, K., Davis, S.J., Yuan, W., Yu, L., Liu, Z., 2019b. Global urban expansion offsets climate-driven increases in terrestrial net primary productivity. Nat. Commun. 10, 5558.

Luo, L., Yan, H., Niu, Z.E., 2018. Comparative analysis on three multi-source remote sensing data fusion models in monitoring farmland productivity. J. Geo-Inf. Sci. 20, 268–279.

McCubbin, S., Smit, B., Pearce, T., 2015. Where does climate fit? Vulnerability to climate change in the context of multiple stressors in Funafuti, Tuvalu. Global Environmental Change-Human and Policy Dimensions 30, 43–55.

Miller, J.D., Hutchins, M., 2017. The impacts of urbanisation and climate change on urban flooding and urban water quality: A review of the evidence concerning the United Kingdom. Journal of Hydrology-Regional Studies 12, 345–362.

Muyen, Z., Moore, G.A., Wrigley, R.J., 2011. Soil salinity and sodicity effects of wastewater irrigation in South East Australia. Agric. Water Manag. 99 (1), 33–41.

Niu, Z.E., Yan, H., Chen, J., Huang, M., Wang, S., 2016. Comparison of crop gross primary productivity estimated with VPM model and MOD17 product in field ecosystem of China. Trans. Chin. Soc. Agric. Eng. 32, 191–198.

Nuarsa, I., As-syakur, A., Gunadi, I., Sukewijaya, I., 2018. Changes in Gross Primary Production (GPP) over the Past Two Decades Due to Land Use Conversion in a Tourism City. ISPRS Int. J. Geo-Inf. 7 (2), 57. https://doi.org/10.3390/ijgi7020057.

Pan, J., Dong, L., 2018. Spatio-temporal variation in vegetation net primary productivity and its relationship with climatic factors in the Shule River basin from 2001 to 2010. Hum. Ecol. Risk Assess. 24 (3), 797–818.

Pan, N., Wang, S., Liu, Y., Hua, T., Zhang, J., Xue, F., Fu, B., 2021. Quantifying responses of net primary productivity to agricultural expansion in drylands. Land Degrad. Dev. 32 (5), 2050–2060.

Pei, Y., Dong, J., Zhang, Y., Yang, J., Zhang, Y., Jiang, C., Xiao, X., 2020. Performance of four state-of-the-art GPP products (VPM, MOD17, BESS and PML) for grasslands in drought years. Ecol. Inf. 56, 101052. https://doi.org/10.1016/j.ecoinf.2020.101052.

Rath, K.M., Rousk, J., 2015. Salt effects on the soil microbial decomposer community and their role in organic carbon cycling: A review. Soil Biol. Biochem. 81, 108–123.

Rudgers, J.A., Chung, Y.A., Maurer, G.E., Moore, D.I., Muldavin, E.H., Litvak, M.E., Collins, S.L., 2018. Climate sensitivity functions and net primary production: A framework for incorporating climate mean and variability. Ecology 99 (3), 576–582.

Salas, E.A.L., 2021. Waveform LiDAR concepts and applications for potential vegetation phenology monitoring and modeling: a comprehensive review. Geo-spatial

Information Science 24 (2), 179–200. https://doi.org/10.1080/10095020.2020.1761763.
Shao, Y., Lunetta, R.S., 2012. Comparison of support vector machine, neural network, and CART algorithms for the land-cover classification using limited training data points. ISPRS J. Photogramm. Remote Sens. 70, 78–87.
Shao, Z., Sumari, N.S., Portnov, A., Ujoh, F., Musakwa, W., Mandela, P.J., 2021. Urban sprawl and its impact on sustainable urban development: a combination of remote sensing and social media data. Geo-spatial Information Science 24 (2), 241–255. https://doi.org/10.1080/10095020.2020.1787800.
Shao, Z., Zhang, L., Wang, L., 2017. Stacked Sparse Autoencoder Modeling Using the Synergy of Airborne LiDAR and Satellite Optical and SAR Data to Map Forest Above-Ground Biomass. IEEE J. Sel. Top. Appl. Earth Obs. Remote Sens. 10 (12), 5569–5582.
Smith, P., House, J.I., Bustamante, M., Sobocká, J., Harper, R., Pan, G., West, P.C., Clark, J.M., Adhya, T., Rumpel, C., Paustian, K., Kuikman, P., Cotrufo, M.F., Elliott, J.A., McDowell, R., Griffiths, R.I., Asakawa, S., Bondeau, A., Jain, A.K., Meersmans, J., Pugh, T.A.M., 2016. Global change pressures on soils from land use and management. Glob. Change Biol. 22 (3), 1008–1028.
Song, J., Wan, S., Piao, S., Knapp, A.K., Classen, A.T., Vicca, S., Ciais, P., Hovenden, M.J., Leuzinger, S., Beier, C., Kardol, P., Xia, J., Liu, Q., Ru, J., Zhou, Z., Luo, Y., Guo, D., Adam Langley, J., Zscheischler, J., Dukes, J.S., Tang, J., Chen, J., Hofmockel, K.S., Kueppers, L.M., Rustad, L., Liu, L., Smith, M.D., Templer, P.H., Quinn Thomas, R., Norby, R.J., Phillips, R.P., Niu, S., Fatichi, S., Wang, Y., Shao, P., Han, H., Wang, D., Lei, L., Wang, J., Li, X., Zhang, Q., Li, X., Su, F., Liu, B., Yang, F., Ma, G., Li, G., Liu, Y., Liu, Y., Yang, Z., Zhang, K., Miao, Y., Hu, M., Yan, C., Zhang, A., Zhong, M., Hui, Y., Li, Y., Zheng, M., 2019. A meta-analysis of 1,119 manipulative experiments on terrestrial carbon-cycling responses to global change. Nat. Ecol. Evol. 3 (9), 1309–1320.
Stocker, B.D., Zscheischler, J., Keenan, T.F., Prentice, I.C., Seneviratne, S.I., Peñuelas, J., 2019. Drought impacts on terrestrial primary production underestimated by satellite monitoring. Nat. Geosci. 12 (4), 264–270.
Sun, Y., Zhang, X., Ren, G., Zwiers, F.W., Hu, T., 2016. Contribution of urbanization to warming in China. *Nature*. Clim. Change 6 (7), 706–709.
Tian, F., Brandt, M., Liu, Y.Y., Verger, A., Tagesson, T., Diouf, A.A., Rasmussen, K., Mbow, C., Wang, Y., Fensholt, R., 2016. Remote sensing of vegetation dynamics in drylands: Evaluating vegetation optical depth (VOD) using AVHRR NDVI and in situ green biomass data over West African Sahel. Remote Sens. Environ. 177, 265–276.
Tran, D.X., Pla, F., Latorre-Carmona, P., Myint, S.W., Caetano, M., Kieu, H.V., 2017. Characterizing the relationship between land use land cover change and land surface temperature. ISPRS J. Photogramm. Remote Sens. 124, 119–132.
Trinder, J., Liu, Q., 2020. Assessing environmental impacts of urban growth using remote sensing. Geo-spatial Information Science 23 (1), 20–39.
Walther, S., Voigt, M., Thum, T., Gonsamo, A., Zhang, Y., Köhler, P., Jung, M., Varlagin, A., Guanter, L., 2016. Satellite chlorophyll fluorescence measurements reveal large-scale decoupling of photosynthesis and greenness dynamics in boreal evergreen forests. Glob. Change Biol. 22 (9), 2979–2996.
Weinzettel, J., Vačkářů, D., Medková, H., 2019. Potential net primary production footprint of agriculture: A global trade analysis. J. Ind. Ecol. 23 (5), 1133–1142.
Weiss, M., Jacob, F., Duveiller, G., 2020. Remote sensing for agricultural applications: A meta-review. Remote Sens. Environ. 236, 111402. https://doi.org/10.1016/j.rse.2019.111402.
Wen, Y., Liu, X., Bai, Y., Sun, Y., Yang, J., Lin, K., Pei, F., Yan, Y., 2019. Determining the impacts of climate change and urban expansion on terrestrial net primary production in China. J. Environ. Manage. 240, 75–83.
Wu, S., Zhou, S., Chen, D., Wei, Z., Dai, L., Li, X., 2014. Determining the contributions of urbanisation and climate change to NPP variations over the last decade in the Yangtze River Delta, China. Sci. Total Environ. 472, 397–406.
Yao, Y., Wang, X., Li, Y., Wang, T., Shen, M., Du, M., He, H., Li, Y., Luo, W., Ma, M., Ma, Y., Tang, Y., Wang, H., Zhang, X., Zhang, Y., Zhao, L., Zhou, G., Piao, S., 2018. Spatiotemporal pattern of gross primary productivity and its covariation with climate in China over the last thirty years. Glob. Change Biol. 24 (1), 184–196.
Yin, X., Zhu, H., Gao, J., Gao, J., Guo, L., Wang, J., 2020. Effects of climate change and human activities on net primary productivity in the Northern Slope of Tianshan, Xinjiang, China. Trans. Chin. Soc. Agric. Eng. 36, 195–202.
Zhang, C., Ren, W., 2017. Complex climatic and CO2 controls on net primary productivity of temperate dryland ecosystems over central Asia during 1980–2014. Journal of Geophysical Research-Biogeosciences 122 (9), 2356–2374.
Zhang, Y., Xiao, X., Jin, C., Dong, J., Zhou, S., Wagle, P., Joiner, J., Guanter, L., Zhang, Y., Zhang, G., Qin, Y., Wang, J., Moore, B., 2016. Consistency between sun-induced chlorophyll fluorescence and gross primary production of vegetation in North America. Remote Sens. Environ. 183, 154–169.
Zhong, Q., Ma, J., Zhao, B., Wang, X., Zong, J., Xiao, X., 2019. Assessing spatial-temporal dynamics of urban expansion, vegetation greenness and photosynthesis in megacity Shanghai, China during 2000–2016. Remote Sens. Environ. 233, 111374. https://doi.org/10.1016/j.rse.2019.111374.
Zhuang, Q., Shao, Z., Huang, X., Zhang, Y., Wu, W., Feng, X., Lv, X., Ding, Q., Cai, B., Altan, O., 2021. Evolution of soil salinization under the background of landscape patterns in the irrigated northern slopes of Tianshan Mountains, Xinjiang, China. *Catena* 206, 105561. https://doi.org/10.1016/j.catena.2021.105561.
Zhuang, Q., Wu, S., Yan, Y., Niu, Y., Yang, F., Xie, C., 2020. Monitoring land surface thermal environments under the background of landscape patterns in arid regions: A case study in Aksu river basin. Sci. Total Environ. 710, 136336. https://doi.org/10.1016/j.scitotenv.2019.136336.